京都大学防災研究所年報 第 58 号 B 平成 27 年 6 月
Annuals of Disas. Prev. Res. Inst., Kyoto Univ., No. 58 B, 2015

Analysis of Breach Characteristics and Equilibrium Scour Pattern for Overtopping Induced River Dyke breach

Pawan Kumar BHATTARAI(1), Hajime NAKAGAWA, Kenji KAWAIKE and Hao ZHANG(2)

(1) Graduate School of Engineering, Kyoto University
(2) Agriculture Unit, Natural Science Clusters, Kochi University

Synopsis

River dykes are important and effective measure to prevent floods.The main consequences on the flood risk due to construction of river embankments or dykes are that, firstly, it increases the flood hazard reducing the lateral flow storage area and hence the flow capacity of peak discharges attenuation and, secondly, the amount of potential damages induced by flooding is dramatically increased, being the surrounding areas often urbanized. Therefore, although the existence of dyke lowers the probability of flooding but the consequences to personal safety and property are much higher should a dyke overtop or fail. The dynamic lateral widening of the breach process, resulting flow and sediment hydrographs and the scour beneath or downstream of dyke are poorly understood in current studies. Therefore, this study conducted laboratory experiments and numerical simulations of river dyke breach due to overtopping flow with different sediment sizes. The influence of sediment size of dyke materials on the breach process were discussed based on the results of the laboratory experiments, and a numerical model was developed to simulate the breach process of dykes by flow overtopping. The developed model introduced the effects of infiltration process and resisting shear stress due to suction of unsaturated sediment as a new expression. To simulate the dyke breach phenomenon, the numerical model consisted of different modules: two-dimensional shallow-water flow, seepage flow, sediment transport using a deterministic model, and collapse model. The reproducibility of the developed model was tested using experimental data on dyke breach phenomena. The numerical results are well agreed with the results of the sandy river dyke experiments.

Keywords: River dyke, Seepage flow, Lateral widening, Suction, Breach discharge, Scour

1. Introduction

River dykes, considered as defense structure, are constructed to prevent flooding of valleys and their inhabitants and confine the flow of the river for higher and faster flow. In this context of work, we refer to dykes as to man- made earthen embankments built along a river parallel to the river flow and flow strikes the dyke length not perpendicularly. River Dykes is an important and effective measure to prevent floods.The main consequences on the flood risk due to construction of river embankments or dykes are that, firstly, it increases the flood hazard reducing the lateral flow storage area and hence the flow capacity of peak discharges attenuation and, secondly, the amount of potential damages induced by flooding is dramatically increased, being the surrounding areas often urbanized. Therefore, although the existence of dyke lowers the probability of flooding but the consequences to personal safety and property are much higher should a dyke overtop or fail. In the context of study, Dyke failure is considered to be the situation where erosion or structural failure of the earthen embankment cause flood water to pass over or through the embankment in an increasingly uncontrolled manner (Morris et. al. 2009), leading to a hole or breach in the dyke.The problem of embankment failures has always been of great

importance because of their disastrous effects. Also, it is important to control the local scour depth under foundation and at downstream of hydraulic structures to ensure safety of these structures But, the study of scour pattern and depth is poorly understood if it comes in the case of dyke foundation and downstream.

Photo 1 Damage in the Kenufuchi River, Hokkaido, Japan (Source: PWRI, Hokkaido)

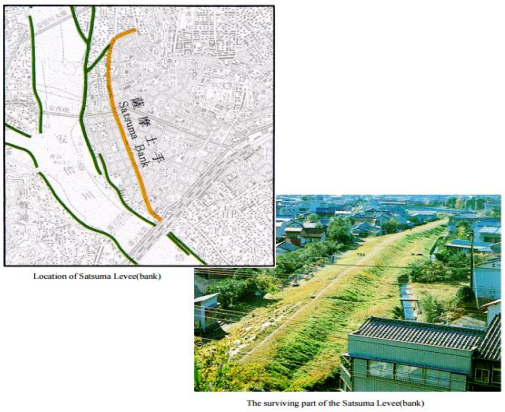

Fig.1 Satsuma Levee, Japan (Source: MLIT, Japan)

In Japan, The first dyke or levee construction date during the reign of Emperor Nintoku mentioned in Nihon-Shoki (first official history of Japan). The levee namely Manda-no-Tsutsumi (Manda Levee) was constructed in Yodo river (Neyagawa city, Osaka Prefecture, Owada). Similarly, The Satsuma Levee (Fig. 1) is said to have been built by the order of Tokugawa Ieyasu to protect the town of Sunpu from floods. The levee was constructed at Abe River (Shizuoka City, Shizuoka Prefecture).

A dyke failure can be either natural or man-made. Natural failures occur due to extreme flood events, earthquakes, soil settlements, piping, seepage, overtopping, or animal burrowing. Man-made causes include e.g. poor construction, incorrect design, improper location, or sabotage. In many cases, a combination of several failure modes leads to the actual dyke failure (See Fig. 3). Dyke overtopping starts normally at the lowest crest elevation or at a local dyke discontinuity, e.g. at a bridge abutment. The shear stresses induced by the water flow over the downstream dyke slope initiate the erosion process. Erosion starts if the induced shear stress exceeds the critical sheer stress of the dyke material. The soil particles are then entrained and transported downstream. Any initial small breach or a local soil settlement represent a crest weakness and may develop into a larger breach resulting in dyke failure.

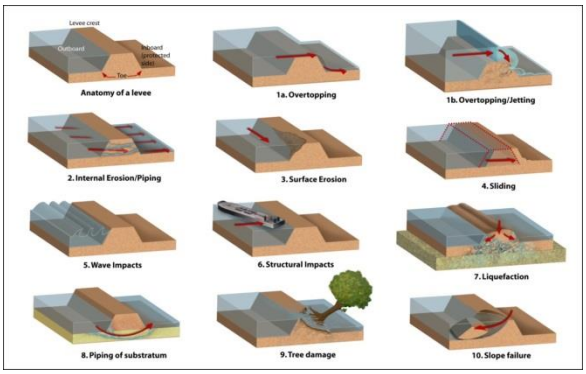

Fig.2 Dyke failure mechanisms (Source: NSF)

Dyke breaching represents a complex interaction between hydraulic, geotechnical and structural processes (See Fig. 2). The breaching process varies with material type and state, hydraulic load and dyke condition. Several distinct stages have been observed and differ especially for cohesive or non-cohesive materials. As the current project is limited to breaches of incohesive dykes due to overtopping, only this process is discussed below. Various model studies in the past investigated both plane (2D) and spatial (3D) breach processes due to overtopping using hydraulic modeling. Further, the evaluation of real case data resulted in additional information on the breach process.

Tsujimoto et al., (2006) studied levee breach process of a river by overflow erosion; they conducted numerical approach for the evolution process of levee using unlike relative height of floodplain to river bed. In Hokkaido, Japan also,

Full Scale overflow breakage tests were first performed using the Chiyoda Test Channel (completed in 2007) to examine the dyke breakage/widening mechanism.

Photo 2 Maruyama river dyke breach (Source: MLIT)

Although several researches have been conducted to understand the embankment dam failure, there has been little focus on river dyke breaching processes and scour under the dyke and the flood plain. The experimental studies to understand overtopping induced embankment failure have been carried out by previous researchers (Powledge et al. 1989, Tingsanchali et al. 2003, Pickert et al. 2011). Powledge et al. (1989) presented the hydraulic aspect of overtopping flow while Tingsanchali et al. (2003) discussed flow patterns and progressive damage and Pickert et al. (2011) showed the cohesion due to pore water pressure influence on stability. The inflow of river water and sediment due to levee breach and the expansion process considering different sizes of levee were conducted by Fujita et al. (1987). Similarly the enlargement of breaches in alluvial plains and the mechanism and hydraulic characteristics were also identified by Fujita and Tamura (1987). The embankment failure, sedimentation over flood plain, field investigation and model study to find out sedimentation process in flood plain were carried out by Islam et al (1994).

Tinsanchali and Chinnarasri (2001) developed a one-dimensional numerical model that considered circular slope stability for embankment failure and compared the simulated results with the experiments. Moreover, Tsujimoto et al. (2006) also studied the dyke breach process by overtopping flow and the erosion process by numerical simulation. Kakinuma et.al. (2013) conducted large scale experiments in which levee breach caused by side overflows from an actual river channel were reproduced using a full-scale model. The authors identified four characteristics breach processes, focusing on levee breach process and side overflow, as well as sedimentation in the flume and overflow area. They also studied briefly about scour mechanism in the flood plain and foundation of levee.

In the last forty years, particularly since the 1980's, many mathematical models have been developed for the simulation of breach growth in embankments. Some models ignore the mechanism of erosion by lumping every possible factor into two principal parameters: final shape and breach formation time (Fread, 1998a; U.S. Army Corps of Engineers, 1981). Other physically based embankment breach models use principles of hydraulics, theory of sediment transport and soil mechanics to simulate the breach growth process and the breach flow hydrograph. The category includes models, e.g. Ponce and Tsivogolu (1981), Fread (1988b), Singh and Scarlatos (1988), Bechteler and Broich (1991), Visser (1988), and Wang and Bowles (2006).

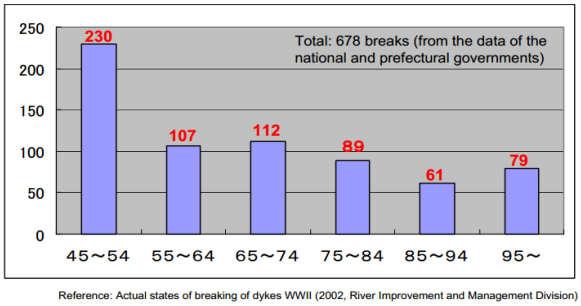

Fig.3 Dyke breaches Scenario in Japan (Source: MLIT)

Several previous studies attempted to use numerical simulation to reproduce the phenomenon of embankment erosion and failure due to overtopping flow. For example, Tingsanchali and Chinnarasri (2001) developed a one-dimensional numerical model that considered circular slope stability for embankment failure and compared the simulated results with the experimental results. They indicated the importance of the estimation of the erosion rate calculated using a sediment transport formula. Several sediment transport models were applied to their model, and the coefficients of the sediment transport model were adjusted by trial and error to fit their experimental data and to investigate the effect of coefficients

related to the erosion rate. Gotoh et al. (2002; 2008) introduced the moving particle semi-implicit (MPS) method, which is classified in a grid less numerical model, a numerical model of embankment erosion that avoids numerical diffusion in water surface tracking.

Many previous studies cover a wide range of parameters regarding hydraulic conditions, dyke designs and sediment properties. Despite this knowledge, the breach process is still poorly understood because only limited test data are available due to a significant laboratory effort. Systematic model tests are scarce and most research is limited to one specific test setup or one specific failure mode. Most results may therefore only be applied to particular problems, e.g. to special dyke configurations or to a particular grain size. Further, new measuring devices to simultaneously determine water surface and sediment profiles were rarely used and are not yet completely established regarding reliability and measuring errors. Most systems were only applied by one specific research team and the overall experience is therefore limited.

Moreover, a lot of numerical simulations of inundation process following to dyke breach has been conducted to make flood hazard maps for almost all rivers with large to meddle scales basins in Japan. In such simulations, levee breach widths and their widening process are very roughly postulated to be proportional to river channel width and visually gathered empirical data. But, they did not consider so much about subsequent phenomena appearing in the river bed and in the floodplain as well as topographic changes over the floodplain during dyke breach. In this research, the attempted have been taken to recognize the dyke breach phenomena and lateral widening process and scour using a numerical simulation scheme and as well as small-scale laboratory experiments.

2. Numerical scheme for dyke breach characteristics

Physically based models such as NWS-DAMBRK (Fread 1988) and NWS-BREACH (Fread 1991) are commonly used to predict the outflow hydrograph of embankment dam (Bajracharya et al. 2007b; Wang et al. 2008; Shrestha et al. 2010). Furthermore, HEC-RAS dam breach model (U.S. Corps of Engineers 2002) is also employed by Osti and Egashira (2009) to predict the outflow hydrograph of glacial lake outburst. The actual mechanism of dam surface slope failure and head cut and lateral dam surface erosion are not considered in available breach models. The failure mechanism and erosion process of river dykes are still not thoroughly understood.

A numerical model for predicting erosion due to overtopping flow at a river embankment was developed by combining four modules: surface flow, seepage flow, sediment transport, and slope failure. The novelty of this study is in the combination of these modules to reproduce the complicated embankment failure process. There are many interactions among the modules, and the highlight of the present model is its estimation of the erosion rate by considering that the effect of resisting shear stress due to suction depends on saturation conditions on the embankment surface, which is calculated using the result from the seepage flow module. In order to focus on the improvement in the treatment of the dyke breach process, the developed model was reduced to vertical two-dimensional calculations in seepage and erosion modules; however, the horizontal 2D flow model was introduced to consider the extensibility for our future work.

2.1 Seepage Model

The seepage flow in the dyke body is caused by the blocked water stage behind the dyke. The transient flow in the dyke body after breaching start in the dyke can be analyzed by Richards' equation (1931). To evaluate the change in pore water pressure in variably saturated soil, pressure based Richards' equation is used (Awal et al, 2007).

$$C\frac{\partial h}{\partial t} = \frac{\partial}{\partial x}\left(K_x(h)\frac{\partial h}{\partial x}\right) + \frac{\partial}{\partial z}\left(K_z(h)\left(\frac{\partial h}{\partial z} + 1\right)\right) \qquad (1)$$

where h is the water pressure head, Kx(h) and Kz(h) are the hydraulic conductivity in x and z direction, C is the specific moisture capacity ($\partial\theta/\partial h$), θ is the soil volumetric water content, t is the time, x is the horizontal spatial coordinate and z is the vertical spatial coordinate taken as positive upwards. Equation represents flow in both the

unsaturated domain as well as in the saturated domain. The unsaturated flow involves a two-phase flow of air and water, however only the flow of the water has been considered, where the air phase is continuous and is at atmospheric pressure, and it does not affect the dynamics of the water phase. Richards' equation is a non-linear parabolic partial differential equation in the unsaturated zone and elliptic in the saturated zone. Line successive over-relaxation (LSOR) is often a very effective method of treating cross-sectional problem grids. LSOR scheme is used in this study for the numerical solution of Richards' equation.

In order to solve Richard's equation, the constitutive equations, which relate the pressure head to the moisture content and the relative hydraulic conductivity, are required. In this study, constitutive relationship proposed by van Genuchten are used for establishing relationship of θ − h and K − θ , with m =1 − (1/ η).

2.2 Flow and Erosion Model

The governing equations of the flow module are the depth-averaged two-dimensional equations and the continuity equation of the flow, which are described as follows:

$$\frac{\partial u}{\partial t}+u\frac{\partial u}{\partial x}+v\frac{\partial u}{\partial y}=-g\frac{\partial H}{\partial x}-\frac{\tau_{bx}}{\rho h}+\frac{\partial}{\partial x}\left(\frac{\tau_{xx}}{\rho}\right)+\frac{\partial}{\partial y}\left(\frac{\tau_{xy}}{\rho}\right) \quad (2)$$

$$\frac{\partial v}{\partial t}+u\frac{\partial v}{\partial x}+v\frac{\partial v}{\partial y}=-g\frac{\partial H}{\partial x}-\frac{\tau_{by}}{\rho h}+\frac{\partial}{\partial x}\left(\frac{\tau_{xy}}{\rho}\right)+\frac{\partial}{\partial y}\left(\frac{\tau_{yy}}{\rho}\right) \quad (3)$$

$$\frac{\partial h}{\partial t}+\frac{\partial(uh)}{\partial x}+\frac{\partial(vh)}{\partial y}=0 \quad (4)$$

where u and v are flow velocity components in x and y directions, g is the acceleration due to gravity, H is the water level, h is the flow depth, and ρ is the water density and τ_{bx} and τ_{by} are the bottom shear stresses in the x and y directions. The shear forces due to turbulenceτ_{xx}, τ_{yy}, τ_{xy} are described as follows;

$$\frac{\tau_{xx}}{\rho}=2\varepsilon\frac{\partial u}{\partial x},\ \frac{\tau_{yy}}{\rho}=2\varepsilon\frac{\partial v}{\partial x},\ \frac{\tau_{xy}}{\rho}=\varepsilon\left(\frac{\partial u}{\partial y}+\frac{\partial v}{\partial x}\right) \quad (5)$$

where ε is eddy viscosity ($\varepsilon=(\kappa u_* h)/6$), κ is von-Karman's constant, and u_* is friction velocity. The bottom shear stresses are expressed as follows:

$$\tau_{bx}=\rho g n^2 u\sqrt{u^2+v^2}\Big/h^{1/3} \quad (6)$$

$$\tau_{by}=\rho g n^2 v\sqrt{u^2+v^2}\Big/h^{1/3} \quad (7)$$

where n is the manning's coefficient. The discretization equations of the flow module are solved by using the SIMPLE revised (SIMPLER) scheme (See Fig. 4), a widely used scheme that utilizes the relationship between velocity and pressure corrections to enforce mass conservation (Patanakar 1980).

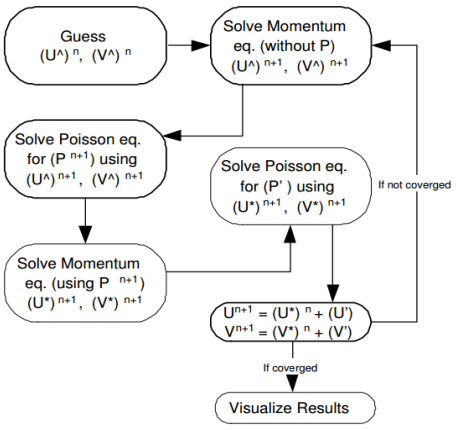

Fig. 4 Flow chart of SIMPLER Scheme

The erodible bed thickness of sandy dyke at each calculation time step may be partly saturated and partly unsaturated. Usually top surface close to the flowing water is saturated (Nakagawa et al. 2011). In saturated region, there is no effect of suction in the soil mass. However, in unsaturated region, the suction effects in the erosion of soil. Therefore, the erosion process of dyke is computed by considering both the saturated and unsaturated erosion mechanism (Nakagawa et al. 2011). The erosion velocity equation given by Takahashi et al. (1992) for unsaturated bed without considering suction is described as

$$\frac{i_{bsat}}{\sqrt{gh}}=K_e sin^{3/2}\theta_b\left\{1-\frac{\sigma-\rho}{\rho}c\left(\frac{tan\phi}{tan\theta_b}-1\right)\right\}^{1/2}\times\left(\frac{tan\phi}{tan\theta_b}-1\right)(c_\infty-c)\frac{h}{d_m} \quad (8)$$

where i_{bsat} is the erosion rate without considering suction, K_e (=0.8) is the erosion rate constant, c_∞ is the equilibrium sediment

concentration, ϕ is the angle of internal friction, θ_b is the slope of the channel and the value of $\tan\theta_b$ in the above equations is used the energy gradient as follows:

$$tan\theta_b = \sqrt{\tau_{bx}^2 + \tau_{by}^2}/(\rho g h) \quad (9)$$

The erosion velocity equation for unsaturated bed considering suction is described as (Nakagawa et al. 2011)

$$\frac{i_{bunsat}}{\sqrt{gh}} = K_e sin^{3/2}\theta_b \left\{1 - \frac{\sigma-\rho}{\rho} c \left(\frac{tan\phi}{tan\theta_b} - 1\right) - \frac{\Delta\tau_{suc}}{\rho g h sin\theta_b}\right\}^{1/2} \times \left(\frac{tan\emptyset}{tan\theta_b} - 1\right)(c_{\infty suc} - c)\frac{h}{d_m} \quad (10)$$

$$\Delta\tau_{suc} = \rho g|\psi|\left(\frac{\theta-\theta_r}{\theta_s-\theta_r}\right)tan\phi \quad (11)$$

where i_{bunsat} is the erosion rate considering suction, $\Delta\tau_{suc}$ is the shear stress increment due to the suction and $c_{\infty suc}$ is the equilibrium sediment concentration considering suction, which is expressed as

$$c_{\infty suc} = \frac{\rho tan\theta_b - \frac{\Delta\tau_{suc}}{gh\cos\theta_b}}{(\sigma-\rho)(tan\phi - tan\theta_b)} \quad (12)$$

The total erosion rate considering both with and without suction effect is expressed as

$$i_b = f \cdot i_{bsat} + (1-f) \cdot i_{bunsat} \quad (13)$$

where f is the variable based on thickness of saturated part of total eroded thickness (0<f<1), and f=0.5 is used as Nakagawa et al. (2011) for the computation.

If sediment concentration in the flow is greater than the equilibrium sediment concentration ($c > c_\infty$), the deposition occurs and the deposition velocity equation is expressed as follows (Takahashi et al. 1992):

$$i_b = \delta_d \frac{c_\infty - c}{c_*}\sqrt{u^2 + v^2} \quad (14)$$

where δ_d (=0.03) is the deposition coefficient. The variation in the embankment shape is expressed as follows:

$$\frac{\partial z_b}{\partial t} + i = i_{sml} + i_{smr} \quad (15)$$

where, z_b is the erosion or deposition thickness of the bed measured from the original bed surface elevation, i_{sml} and i_{smr} are the mean recessing velocity of the left and right hand side banks of the incised channel respectively.

Lateral erosion velocity is assumed as a function of the shear stress on the side wall assigned by the interstitial fluid of the overlying sediment-laden flow τ_{sf}. The value of τ_{sf} is then assumed as the half of the bed shear stress τ_f. One may write the recession velocity of the wetted sidewall under the surface of the flow i_s as

$$\frac{i_s}{\sqrt{gh}} = \left(\frac{1}{2}\right)^{1.5} K_e sin^{3/2}\theta_b \left\{1 - \frac{\sigma-\rho}{\rho} c \left(\frac{tan\phi}{tan\theta_b} - 1\right) - \frac{\Delta\tau_{suc}}{\rho g h sin\theta_b}\right\}^{1/2} \times \left(\frac{tan\emptyset}{tan\theta_b} - 1\right)(c_{\infty suc} - c)\frac{h}{d_m} \quad (16)$$

where K_e is a constant. By recession of the wetted sidewall, the part of the wall upward of the surface of the flow may lose its stability and fall into the flow. If one assumes the recession of the whole sidewall is parallel as shown in Figure 5, the mean recession velocity of the side walls would be

$$i_{sml} = \frac{h_l}{l_l + h_l} i_{sl} \ , \ i_{smr} = \frac{r}{l_r + h_r} i_{sr} \quad (17)$$

The finite difference calculation of the system of equations referred to above on the two dimensional rigid grid system set on the horizontal plane requires a little contrivance, because on such grid the channel can enlarge its width only discretely in spite of the actual continuous widening. To overcome this problem, one may assume that the sediment produced by the recession of banks, e.g. $i_{smr} = (z_{bs} - z_b)\Delta t$ is supplied only to the cell adjacent to the bank, e.g. cell A in Fig. 5, and it instantaneously raises the elevation of that cell to be eroded by the flow in the channel in the next time step. The channel width is considered not to be changed until the total volume of the sediment supplied, for example, to the cell A becomes equal to the volume of the sediment in the side bank cell at the beginning of the side bank erosion, t_0. At the moment when the two respective volumes of sediment become equal, the channel is considered to be widened by one cell width and the bottom elevation of the new cell adjacent to the new bank is set to be equal to that of the former adjacent cell at time t0. The formulation of the procedure is as follows:

$$\int_{t_o}^{t} i_{sr} h_r \Delta x dt = (z_{bs} + z_{so} - z_b - z_o)|_{t=t_o} \Delta x \Delta y$$

$$\xrightarrow{yields} z_b = z_b|_{t=t_o} \quad (18)$$

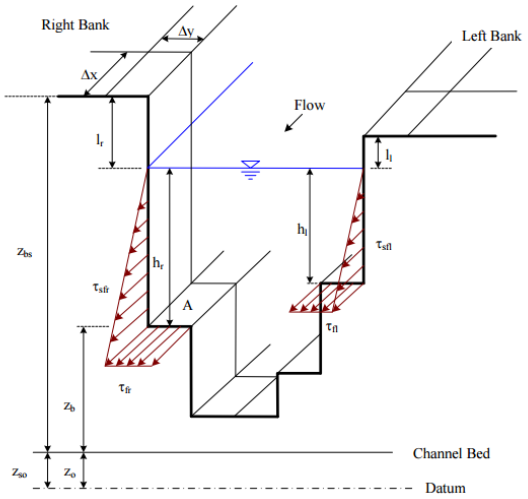

Fig. 5 A cross-section of the incised channel on a dam (Adapted from Takahashi Tomatsu)

2.3 Side channel collapse model

At the place, where the side channel gradient is equal to the angle of repose, it is assumed that a collapse occurs. If the difference in level between two places on the river bed exceeds $\Delta Z_{max} = \Delta x \tan\varphi$, the side channel collapses and the sediment with a volume of ΔVi including the volume of pores move from the calculation point i to the point i+1 (Fig. 6). The collapse sediment volume, ΔVi, is described as (Takahashi et al. 2001)

$$\Delta V_i = \frac{z_i - z_{i+1} - \Delta z_{max}) B_i B_{i+1}}{B_i + B_{i+1}} \Delta x \quad (19)$$

where zi and $zi+1$ are the bed level at the calculation points i and $i+1$, B_i and B_{i+1} are the width of the channel at the calculation points i and $i+1$, and Δx is the distance increment of the calculation points.

2.4 Numerical Simulation parameters

The meshes used for the calculation of surface flow and seepage belong to structured mesh, and the resolution of the computational mesh was set to

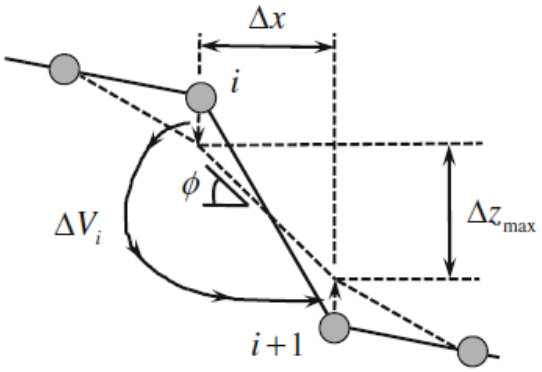

Fig. 6 Transfer of material due to collapse

dx=1.0 cm in the embankment body region and to dx=2.0 cm in other regions of the entire flume area; to dy=1.0 cm in transverse direction for the calculation of flow; and to dx=1.0 cm and dz=0.5 cm for the calculation of seepage flow inside the embankment. Soil parameters for different sands used in these calculations were determined by laboratory experiments conducted by Nakagawa et al. (2011).

3. Experimental methods

The experimental flume was prepared considering realistic orientation of dyke in relation to river flow i.e. the dyke structure was placed parallel to the river flow with the flow direction towards dyke non-perpendicular. The plan and section view of the flume and the picture of setup without the sand dyke are as shown in Fig. 7, Fig.8 and Photo 3 respectively below. The flume was made with acrylic plastic materials with the total length of 4m, out of which, only middle 1 m was made movable dyke while other portions were made fixed.

The main hydraulic test conditions assumed in the current research include: 1) Trapezoidal shaped River and Dyke, 2) Three types of homogenous non-cohesive sediments (Fig. 9 and Table 1), 3) 10% moisture content by weight was added initially to dyke materials and compacted using a similar procedure throughout all the experiments, 4) No core layer or protection was added, 5) Steady inflow with downstream gated weir control, 5) Optical recording by video, high-speed camera and

laser equipment for the scour pattern measurement. The intake is equipped with pump connected supply tank with water collector chambers with flow straightener to generate undisturbed flow from the underground tank with a pump that circulates water continuously between upstream and downstream.

All experiments were conducted using a constant flow discharge in a flume referred to as the inflow. The dyke material was initially provided with 10% moisture content by weight and thoroughly mixed and then compacted with the help of a tamping plate and cylindrical small roller by spraying water layer by layer until about approx. 90% compaction

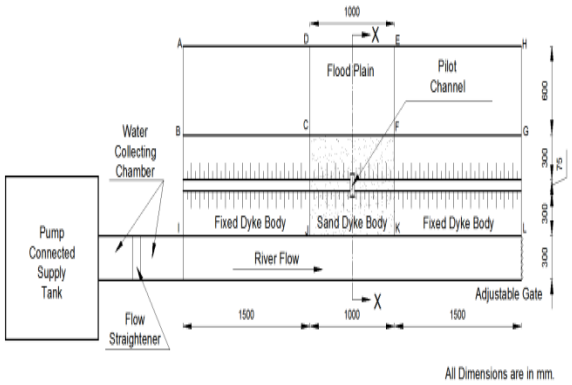

Fig.7 Plan view of Laboratory Set up

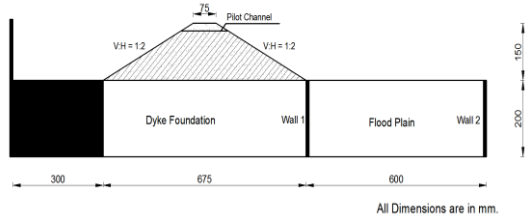

Fig.8 Cross-section along X-X shown in fig.6

was achieved. The inflow was added rapidly to attain a steady state before overtopping started. The flow overtopped the dyke from the pilot channel thus resulting in the lateral widening of the breach from that point. The detail experiment plans with number of experiments are shown in Table 1. For Plan A, a total of 9 experiments and for plan B, 12 (6 each for two scenarios) experiments were conducted for three sediment types.

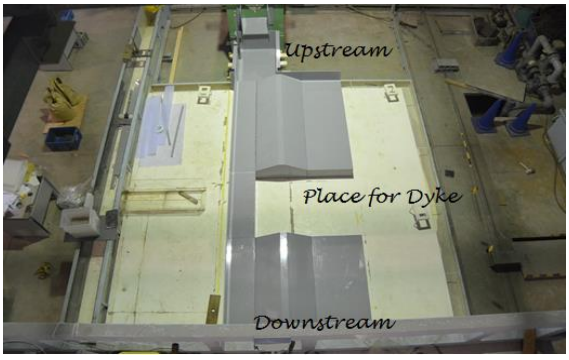

Photo 3 Experimental flume bird's eye view

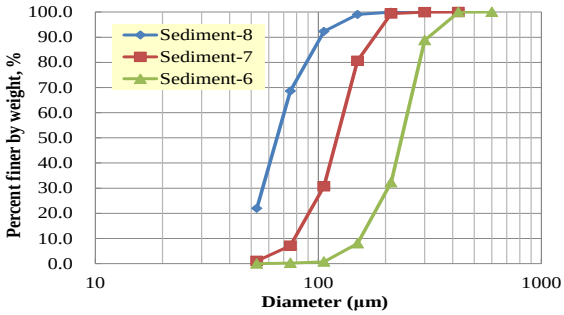

Fig.9 Particle size distribution of sediments

Table 1 Sediment Properties

Sediment type	No.6	No.7	No.8
Sat. moist. content, θs	0.319	0.351	0.400
Resd. moist. content, θr	0.061	0.095	0.117
α	3.837	2.552	1.107
η	3.852	4.148	2.254
Specific gravity, Gs	2.65	2.65	2.65
Mean size, D50 (mm)	0.314	0.166	0.089
Ang. of repose, Φ	34	34	34

Each experiment was repeated three times for plan A and two times for plan B to observe the effect of repeatability.

For experiment plan 'Á' case, the wall 1 and wall 2 were placed and the dyke foundation and flood plain portion were made fixed considering only the movable dyke body (See Fig. 8). The parameters investigated include: Flume discharge Q = 10 liters per sec, dyke height H = 0.15 m, dyke length L = 0.3 m, dyke crest width b = 0.075m (0.5H), and particle size = No.6, No. 7 and No. 8 (See Fig. 9). The upstream and downstream both

dyke slopes are 1:2 (V: H) resulting in a total dyke width of B = 2H+0.5H+2H =4.5H. The pilot channel is made at the center of the 5 cm x 2 cm dyke as a point for the initiation of breach at the desired location. Once the overtopping start and the pilot channel starts to widen laterally, the discharge was measured at the end of the dyke point with the help of collecting water by plastic boxes at certain intervals simultaneously. Such boxes were weighed and computed the discharge by knowing the time intervals for collecting water for each boxes by optical measurement. The entire process of lateral widening was filmed by top and frontal video camera. The dynamic widening processes were directly derived from the camera records.

For Experimental Plan B, two scenarios were studied:

1) Scenario 1: Dyke body, foundation and flood plain all are movable (Representing the areas where the dyke is not strong enough to resist overtopping failure and farm or utility lands in the flood plain)

2) Scenario 2: Dyke body and foundation are fixed but flood plain is made movable (Representing the areas where the dyke is strong enough to overcome failure but the flood plain has populations or farm lands.

For Scenario 1, the wall 1 was removed while wall 2 was placed and the dyke body, foundation and flood plain portions were made movable. Then the breach discharge and the scour pattern after some reference point of time (time when the upstream portion of dyke remained around 10 cm, considering as equilibrium condition) were measured. The pilot channel was still used in this case. The equilibrium bed profile was measured from the Keyence laser profiler.

4 Verification of model with experimental results

4.1 Lateral Widening Process

The overflow rate increased little at the initial overflow stage but begin to increase more when the dyke breakage widened. After the rate peaked, the water level remained almost the same for some time. Since the dyke material is unsaturated, therefore the suction pressure plays a greater role for the stability of almost vertical slopes two sides of pilot channel.

Fig. 10 shows the observed flow regime for the dyke breach analysis. The figure shows the hydrological regime from the channel strikes the downstream end of dyke in an angle developing stagnant region at upstream region. The dyke is always eroded by the main stream of flow passing through the actual flow width and asymmetrical propagation is observed as dyke breaching progressed. The frontal part (downstream part) is eroded continuously while the upstream part, the erosion stops after some time. The lateral widening pattern is quite different to the results obtained when the dyke was placed perpendicular to the flow (like a dam breach) i.e. the widening pattern followed symmetry (Bhattarai et al. 2014). For all sediment sizes, the lateral widening process follows following four phases (See Fig. 11 below):

1) Vertical undermining phase (VUP)

Table 2 Experimental Plan

Experiment Plan	Experiment Type	Sed. No.	Mean Diameter(mm)	No. of Experiments
PLAN A (Breach Characteristics)	Dynamic Lateral Widening	6	0.314	3
	Breach and sediment	7	0.166	3
	Hydrograph	8	0.089	3
PLAN B (Scour Pattern)	a) Scenario 1 Movable dyke, foundation and Flood plain	6	0.314	2
		7	0.166	2
		8	0.089	2
	b) Scenario2 Fixed Dyke and Foundation but Movable Flood Plain	6	0.314	2
		7	0.166	2
		8	0.089	2

The crown of the dyke and downstream slope (slope towards flood plain) area were eroded slowly after overtopping starts the widening did not proceed but vertical undermining of the pilot channel start till it reached toe of the dyke. This process is named as Initiation of dyke erosion. The breach discharge was slow in this stage. This stage remains long for the finer sediment size (sed 8) while as the sediment sizes became coarser, this stage ceased fast.

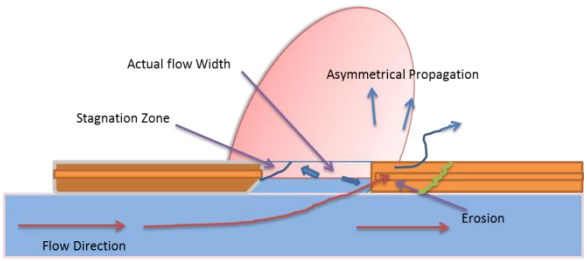

Fig. 10 Flow regime during breaching

2) Initiation of lateral widening Phase (ILWP)

When the vertical undermining reached the toe, the cross-section was eroded rapidly at toe first and then at top of dyke. The dyke widening progressed in both upstream and downstream directions. The middle of the dyke expands less in comparison to top and toe in this stage. Due to skewed flow direction, asymmetrical widening proceeds

3) Lateral widening acceleration phase (LWAP)

Once the initiation of widening occurred, the erosion rate increased rapidly and the breach discharge also increased accordingly. The downstream part was now severely damaged than the upstream one.

4) Widening Deceleration cum stable phase (WDSP)

Once the most of the dyke portions were eroded and the stream width through the dyke increased, the breach discharge started to decrease and become stable but there was still very slow widening proceeding downstream but surprisingly, the upstream portions seem stable.

In summary, for all sediment sizes, the nature of the curve remains same except the rate of erosion i.e. erosion of dyke takes little longer time for finer sediment than coarser one. It shows an important impact of sediment size.

Fig. 11 Four phases of lateral widening process (Top left-1, Top right-2, Bottom left-3 and bottom right-4)

Finer the sediment size, higher the development of suction pressures due to unsaturated condition which finally develops resistance against failure so the finer sediments reluctant to faster erosion. Hence the times taken to reach similar final condition for various sediment sizes are different; finer having late. The middle part of the dyke acts like a hinge as top and bottom of dyke already eroded in some extent.

4.2 Breach and Sediment hydrographs

A numerical simulation of laboratory experiments on embankment erosion was carried out using the developed numerical model. Notch of the width 5cm and depth 2 cm was incised at the crest of the dyke body at the center and the erosion of the surface of the dyke body was observed by optical measurements. The overtopping flow incised a channel on the slope of the dam and that channel increased its cross-sectional area with time caused by the erosion of released water. The breach discharge increases rapidly after the initial overtopping until the maximum value is attained.

The graph clearly shows that time lag of peak of the hydrograph increases with increase in sediment number i.e. decreasing mean diameter of sediments. During breach formation, breach enlargement proceeded rapidly below the water surface in the breach channel. Above the water level there was some apparent cohesion added by water content and adhesion so the side wall was very steep and undermines the slope. The erosion process continues until slope stability was encountered. The slope failure of channel bank around crest of the dam is one of the main causes of higher peak discharge in the experiment compared to simulation.

Fig. 13 shows the comparison of numerical and experimental results and the results shows relatively well correlated. The peak discharge is underestimated by model due to collapse nature of failure and uncertainty in material properties (degree of compaction, mixing of sediments etc.) of the dyke body. Figure 14 shows the sediment discharge for various sediment sizes. The important characteristics of this curve is the graphs have more than one peaks which reveals that the vertical stable wall at the side of the pilot channel falls into the

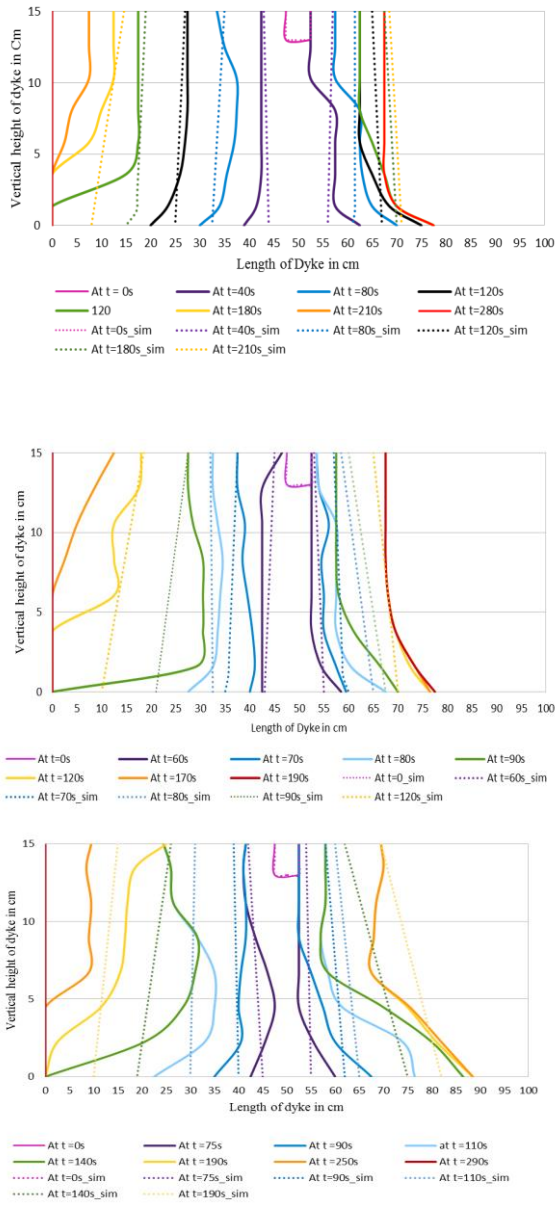

Fig. 12 Lateral widening process (Top: Sed.6, Middle Sed. 7 and Bottom Sed. 8)

center of the breach intermittently. As previously stated, here also sediment no. 8 seems more resistive than other sediments.

5. Experiment result Plan B

5.1 Scenario 1

Scouring may be defined as the removal of material around embankments caused by flow acceleration and turbulence near embankments. Scour has been the major concern for safety of hydraulic structures.

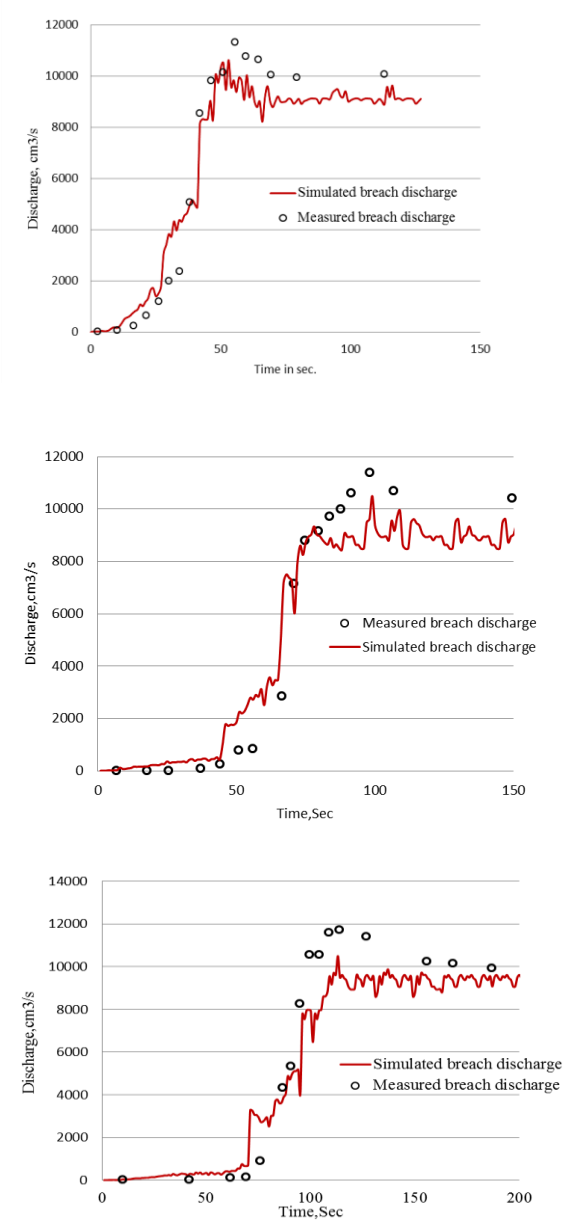

Fig. 13 Breach hydrographs (top: sed. 6, middle: sed. 7 and bottom: sed. 8)

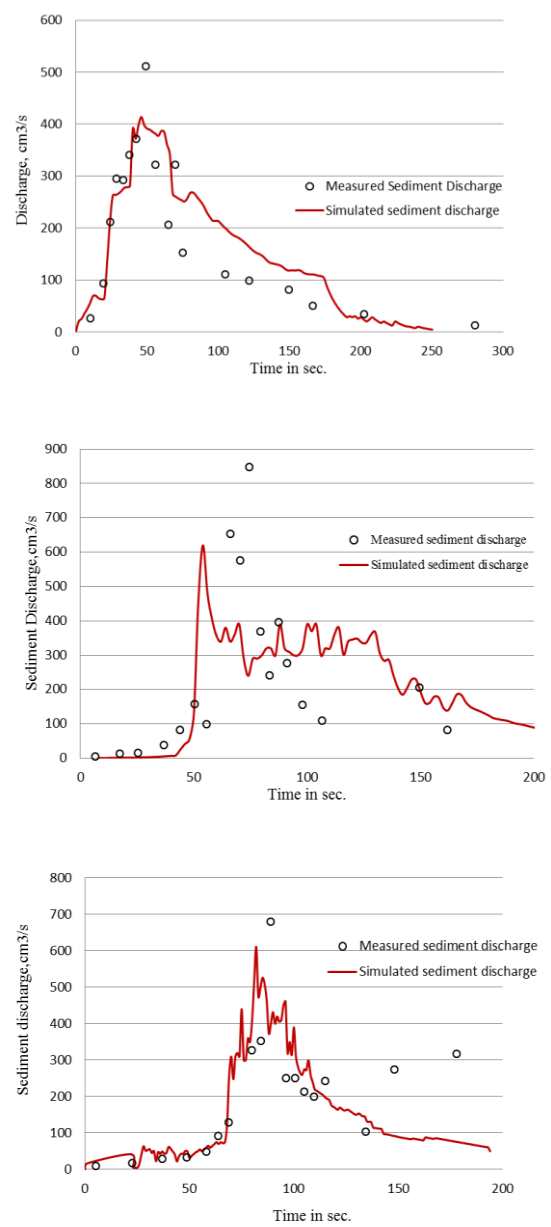

Fig. 14 Sediment hydrographs (top: sed. 6, middle: sed. 7 and bottom: sed. 8)

A large number of hydraulic structures failed as the local scour progresses which gradually undermines the foundations. It is important to control the local scour depth under foundation and at downstream of hydraulic structures. But, the study of scour pattern and depth is poorly understood if it comes in the case of dyke foundation and downstream.

As dyke breach progressed, the channel bed upstream of the broken part underwent scouring due to shear stress applied by the flow. Fig. 15 shows the bed shape after the end of flow as determined using laser measurement for scenario 1 in which case dyke body, foundation and flood plain all are movable. The flow velocity vectors were also determined by PIV method to observe the flow regime which was also plotted overlapping with the scour figure. From the figure, it can be inferred that the maximum scour depth occurred in between the center of dyke and toe. As the sediment size became finer, more scour depth was seen to form.

The analysis shows that the maximum scour depth follows approximately linear relation with the sediment size which needs to be verified with more data in near future. The Fig. 16 shows the linear relation between dimensionless sediment size (ratio between mean diameter of sediment and maximum

foundation depth with same materials below the dyke) and dimensionless maximum scour depth (ratio between maximum scour depth and the maximum foundation depth below the dyke). The graph is only representative one; more data will be needed to give a concrete equation for the relation.

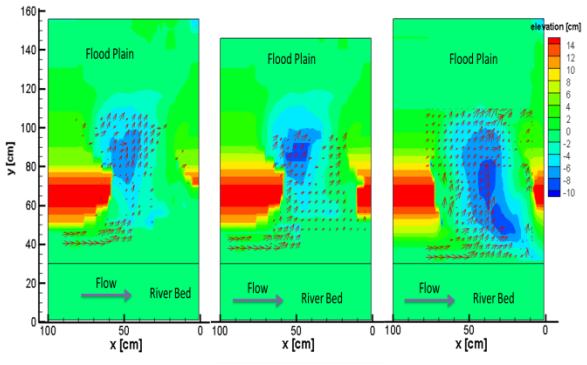

Fig. 15 Equilibrium Scour Pattern overlapped with flow velocity vectors (by PIV) for Sediment 6, 7 and 8 respectively

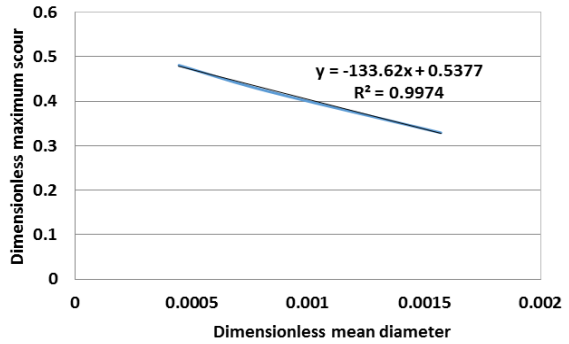

Fig. 16 Relation between maximum scour depth and sediment size

The ripples and dunes of various dimensions are observed in the flood plain because of the fine bed materials. The deposition pattern in the flood plain indicates that initially the flow diverted towards right side of the flood plain but later due to exposition to the deposited sediment the flow travels all along the flood plain. The experiments were also performed for the nearly full saturation of foundation material; the results seem no difference than the previous one; only difference found was the time taken to reach the same equilibrium position. The time was short for the saturated case than unsaturated cases. The concept of hydrographs namely supply hydrographs, breach hydrographs and river hydrographs are also shown in Fig. 17.

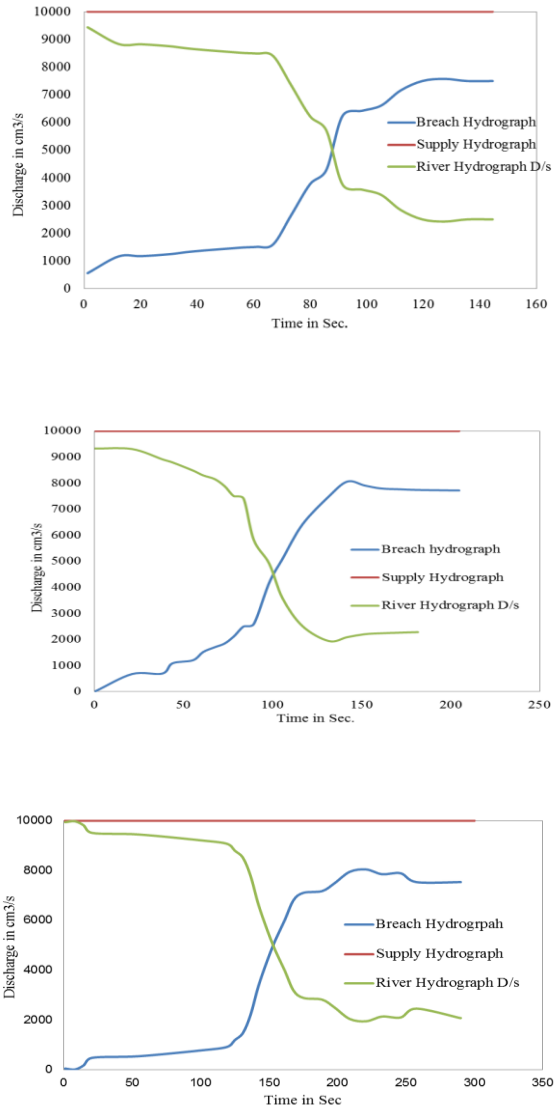

Fig. 17 Hydrographs for scenario 1 (top: sed. 6, middle: sed. 7 and bottom: sed. 8)

5.2 Experimental results: Scenario 2

The scenario 2 experiments were performed by making dyke body and foundation fixed and flood plain only movable. The breaching process was started with the inflow discharge from upstream and the process continues till the equilibrium condition was reached and the measurements were done after the process reached equilibrium state and the results are shown in Fig. 18 in terms of laser measurement of bed morphology after the equilibrium state was reached by the same discharge used in the previous case.

In this case there was no pilot channel and the dyke was overtopped from the whole length. The result also shows similar trend like the scenario 1. The finer the sediments, more large the maximum

scour depth. The location of maximum scour depth is just near the toe for all the cases and the flood plain has no erosion but little deposition or formation of small ripples and dunes. In this case, the process was similar to the scour developed by spillways and due to scouring at the toe, the foundation was exposed, so that there will be danger of failure of hydraulic structure, even though the dyke is strong enough to resist overtopping flow.

In this case also, the finer the particles, the depth of scour became larger. Hence, it can be shown that particle size of dyke materials are very much important regarding the breach or scour phenomena. Hence, the dyke materials should be chosen carefully with sufficcient knowledge of its behaviour during breach process.

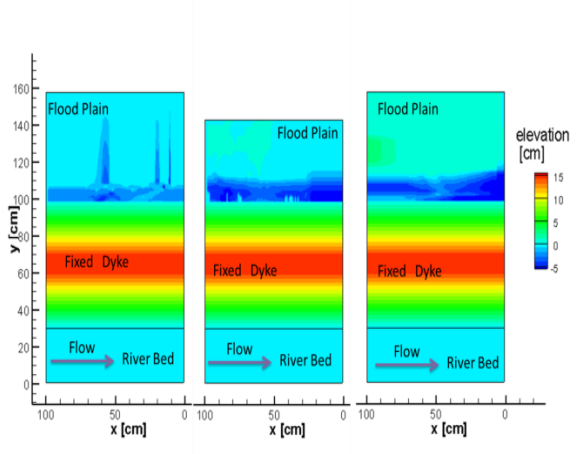

Fig. 18 Equilibrium Scour Pattern for Sediment 6, 7 and 8 respectively

6. Conclusions

The present experimental work investigated the breach characteristics (lateral widening and hydrographs) and scour pattern at the foundation of dyke for various scenarios with the variation of different sediment sizes due to overtopping. A simple but realistic dyke model was used consisting of homogenous uniform materials of various sediment sizes. A steady inflow scenario was tested and all the processes were recorded optically and with laser measurement system. Within the range of test parameters, the dyke breach process was accelerated with the increase in the mean diameter of the particle. For coarser sediments, due to quick saturation of the dyke body, the collapse time decreased. The width of the breach increased at the top and toe section compared to the middle section which acted as a hinge point. In the final stage, middle section also failed leading to the entire dyke collapse.

The downstream dyke portion is more vulnerable as due to the flow angle the downstream part always eroded till the equilibrium condition will reach but for upstream part, the equilibrium condition will reach far early than the later one. So, the four phases of the dyke breach phenomena was observed. The breach discharge and sediment discharge showed the time lag and peak according to the sediment sizes.

The numerical simulation was performed which shows quite good agreement in the case of breach hydrograph, sediment hydrograph and lateral widening process.

The scour pattern is also following a trend with regards to materials forming the dyke and the foundation. The finer the materials, more vulnerable to the scouring were observed. The breach discharge measurement during scour experiment shows that 80% of the total supply discharge passes through the breach area and rest passes as river discharge downstream.

After hydraulic and physical mechanism of dyke breach process are understood, this experimental flume can be adapted to account for further parameters affecting the dyke breach such as surface protection, cohesive materials, core layers, compaction or soil moisture content. The current findings have to be expanded in the next stage.

Acknowledgements

The research is supported by JST/JICA SATREPS Program on disaster prevention/mitigation measures against floods and storm surges in Bangladesh (PI: Dr. Hajime Nakagawa). We would like to express our immense gratitude to Disaster Prevention Research Institute (DPRI) for its cooperation by supporting the lead author by Research Assistant (RA) Fund. The authors are also grateful to the GCOE-ARS program (Sustainability/Survivability Science for a

Resilient Society Adaptable to Extreme Weather Conditions) of the Disaster Prevention Research Institute, Kyoto University, for providing partial financial support. This research was also partially funded by the Japan Society of Promotion of Science, Grant-in-Aid for Scientific Research (B) 22360197.

References

Awal, R., Nakagawa, H., Kawaike, K., Baba, Y. and Zhang, H.: An integrated approach to predict outflow hydrograph due to landslide dam failure by overtopping and sliding, Annual Journal of Hydraulic Engineering, JSCE, Vol. 52, pp.151-156. (2008)

Bhattarai, P.K., Nakagawa, H., Kawaike K. and Zhang H. (2014). Experimental study on river dyke breach characteristics due to overtopping flow. Journal of Japanese Society of Natural Disaster Science, Vol.33, pp 65-74.

Chinnarasri, C., Tingsanchali, T., Weesakul, S. and Wongwises, S. (2003). Flow patterns and damage of dike overtopping. International Journal of Sediment Research 18(4), 301-309.

Fread, D.L. (1998a): The NWS DAMBRK model: theoretical and background/user documentation, National Weather Service (NWS) Report, NOAA, Silver Spring, Maryland, USA.

Fujita Y. and Tamura, T. (1987). Enlargement of breaches in flood levee on alluvial plains. J. of Natural Disaster Science 9 (1), pp 37-60.

Gotoh, H., Ikari, H., Tanioka, H. and Yamamoto, K. (2008). Numerical simulation of river embankment erosion due to overflow by particle method. Annual Journal of Hydraulic Engineering, JSCE, 52, pp 979-984.

Islam M. Z., Okubo K., Muramoto Y. and Morikawa H. (1994). Experimental study on sedimentation over the flood plain due to river embankment failure. Annual of Disaster Prevention Research Institute, Kyoto University. 44 (2), pp 69-92.

Islam M. Z., Okubo K., Muramoto Y. and Kakinuma T., Tobita D., Yokoyama H. and Takeda A. (2013): Levee Breach Observation at Chiyoda Experimental Flume..Advances in River Sediment Research, Taylor and Francis Group. Pg. No. 105

MacDonald, T. C., and Langridge-Monopolis, J. (1984):‘‘Breaching characteristics of dam failures.’’ J. Hydraul. Eng., 110(5), pp. 567–586.

Morris, M.W., Hassan, M., Kortenhaus, A. and Visser, P.J. (2009): “Breaching processes, a state of the art review”. FLOODSITE Report T06-06-03.

Nakagawa, H., Mizutani, H., Kawaike, K., Zhang, H., Yoden Y. and Shrestha B.(2013) ”Numerical Modelling of Erosion of Unsaturated River Embankment due to overtopping Flow” Advances in River Sediment Research, Taylor and Francis Group, London.

Nakagawa, H., Utsumi, T.,Kawaike, K., Baba, Y. and Zhang, H. (2012): “Erosion of Unsaturated embankment due to overtopping water. J. Japan Society of Civil Engineers. Ser. B1 (Hydraulic Engineering).67 (4): II_1-II_4

Patankar, S. V. (1980). Numerical heat transfer and fluid flow. Hemisphere, Washington DC,197.

Powledge, G.R., Ralston, D.C., Miller, P., Chen, Y.H., Cloppner, P.E. and Temple, D.M. (1989a). Mechanics of overflow erosion on embankments I: Research activities. Journal of Hydraulic Engineering 115(8), pp 1040-1055.

Pickert, G., Weitbrecht, V. and Bieberstein, A. (2011): Breaching of overtopped river embankments controlled by apparent cohesion. Journal of Hydraulic Research, 49(2), pp 143-156.

Ponce, V.M. and Tsivoglou, A.J. (1981): Modelling gradual dam breaches, Journal of Hydraulic Division, Vol. 107(7), pp.829-838.

Rabindra Osti and Shinji Egashira (2009): Hydrodynamic characteristics of the Tam Pokhari Glacial Lake outburst flood in the Mt. Everest region, Nepal, Hydrological Process, Vol.23, pp. 2943-2955.

Schmocker, L. (2011): “Hydraulics of dike breaching”. PhD Dissertation, VAW-Mitteilung 218, R.M. Boes, ed. ETH Zurich, Zurich.

Schmocker, L. and Hager, W.H. (2009): ”Modeling dike breaching due to overtopping” J. Hydraulic Res. 47(5), pp. 585‑597.

Singh, V.P. and Scarlatos, P.D. (1988): Analysis of gradual earth-dam failure, Journal of Hydraulic Engineering, Vol.114(1), pp.21-42.

Tingsanchali, T. and Chinnarasri, C. 2001.

"Numerical Model of dam failure due to overtopping" Hydrological Sci. J. 46(1): pp. 113-130.

Van Genuchten, M.T. (1980): A closed-form equation for predicting the hydraulic conductivity of unsaturated soils. Soil Science Society of American Journal, 44, pp 892-898.

Visser, P.J., Zhu, Y. and Vrijling, J.K. (2006): Breaching of dikes. 30th Int. Conf. Coastal Engineering, San Diego CA, pp 2893-2905.

Wang, Z.G. and Bowels, D.S. (2006): "Three dimensional non-cohesive earthen dam breach model. Part 1: Theory and methodology", Advances in Water Resources, Vol.29, pp.1528-1545.

(Received June 11, 2015)